Available online at www.sciencedirect.com
ScienceDirect
Journal of the European Ceramic Society 31 (2011) 493–499
www.elsevier.com/locate/jeurceramsoc

Creep behaviour of tubular $Ba_{0.5}Sr_{0.5}Co_{0.8}Fe_{0.2}O_{3-\delta}$ gas separation membranes

B. Rutkowski, J. Malzbender*, T. Beck, R.W. Steinbrech, L. Singheiser

Forschungszentrum Jülich GmbH, IEF-2, 52425 Jülich, Germany

Received 27 July 2010; received in revised form 13 October 2010; accepted 27 October 2010
Available online 20 November 2010

Abstract

The creep behaviour of $Ba_{0.5}Sr_{0.5}Co_{0.8}Fe_{0.2}O_{3-\delta}$ (BSCF) membrane material was investigated in the temperature range 600–950 °C using tubular specimens. Oxygen partial pressure (4 and 2×10^{-6} mbar), as well as compressive stress (20–63 MPa) were varied. The steady state strain rates from compressive creep tests under axial loading were described by a standard creep equation considering as exponential fitting parameters the influence of temperature, stress, oxygen partial pressure and grain size. Differences in activation energy in the low and high temperature regime appeared to be associated with the disappearance of a second phase. After the creep tests, no significant changes in grain morphology were observed. In addition to the compressive tests, C-ring shaped specimens were machined from the tubes and deformed at 900 °C in a combined tensile-compressive creep mode that revealed the formation of pores along grain boundaries normal to the local tensile stresses that ultimately might lead to creep rupture.

Keywords: Creep; Ceramics; Perovskite; BSCF; Gas separation

1. Introduction

The increasing environmental awareness during the last decade has raised serious questions on the impact of manmade emissions on the global climate changes. The emission of carbon dioxide appears to have been identified as one of the major influence factors. In fact, one of the largest CO_2 emission sources are coal fired power plants. To reduce CO_2 emission by separation of carbon dioxide and subsequent deposition in geological cavities, several power plant concepts are currently exploited.[1] However, they all have in common a loss of efficiency in energy conversion. In this respect the lowest reduction is expected from the so-called OXYFUEL process which is based on the combustion of fossil fuel in oxygen. Furthermore, energy savings are predicted when using inorganic gas separation membranes rather than cryogenic separation techniques to generate the oxygen.[1]

Oxygen can be extracted from the air at elevated temperature by oxygen transport ceramics. Perovskites with "mixed ion electron conducting" (MIEC) properties and a high oxygen permeation coefficient are well suited for the envisaged membrane function. Various perovskites of ABO_3 – type have been suggested as possible material options for this application. $Ba_{0.5}Sr_{0.5}Co_{0.8}Fe_{0.2}O_{3-\delta}$ (BSCF) with high oxygen permeation rate appears the functionally most promising material to date.[2,3] However, under the severe conditions of real application the material's stability is challenged by the high operation temperature, aggressive environments and pressure gradients across the membrane.[4,5] Hence both, microstructural stability and mechanical integrity are also main requirements to warrant the long term functionality of the component. An important thermomechanical aspect at elevated temperatures is the resistance of the perovskite against creep, which determines deformation and ultimately damage. Therefore it is important to quantify and, if necessary, to improve the creep resistance of the ceramic membrane materials.

The creep behaviour of several perovskite structured materials was investigated during recent years.[6–10] $BaCe_{0.8}Y_{0.2}O_{3-\alpha}$ mixed conductors have been reported to deform by diffusional grain boundary sliding mechanism at temperatures between 1200 and 1450 °C.[6] Activation energy and stress exponent were determined to 343 kJ/mol and 1.1, respectively, while strain rates varied from 2×10^{-6} to 5×10^{-4} s^{-1}. In fact, stress exponent changes were also claimed for $SrCo_{0.8}Fe_{0.2}O_{3-\delta}$.[9] The value changed from $n \approx 1$ for stresses between 10 and 20 MPa to

* Corresponding author. Tel.: +49 2461616964; fax: +49 2461613699.
E-mail address: j.malzbender@fz-juelich.de (J. Malzbender).

0955-2219/$ – see front matter © 2010 Elsevier Ltd. All rights reserved.
doi:10.1016/j.jeurceramsoc.2010.10.030

$n \approx 2.5$ for stresses between 40 and 50 MPa. This change has been related to the appearance of a dislocation creep mechanism. The activation energy was reported to be 474 kJ/mol for the grain boundary diffusion and 303 kJ/mol for lattice diffusion.

Acceptable creep rates in a compressive mode for engineering ceramics are reported to be about $10^{-10}\ s^{-1}$, which permits a strain of about 1% per year.[11] Nevertheless, compared to the number of reports on functional aspects, there is still a deficiency in the field of mechanical testing of BSCF membranes.[12,13] Hence, the characterization of the creep behaviour of BSCF based dense ceramic MIEC membranes was defined as an important task in the research alliance "MEM-BRAIN" of the Helmholtz Association of German Research Centres.[1]

In this context, the aim of the current work is to present compressive creep results of tubular BSCF membranes under different atmospheres (air, 20 mbar, 5×10^{-5} mbar total pressure) in a wide range of temperatures (600–950 °C). The steady state creep rate was evaluated and mathematically described by a standard multi-parameter creep equation, linking the creep deformation to temperature, stress, oxygen partial pressure and grain size.

In contrast to the test procedure applied in Ref. 12, in the present study creep tests were performed at constant load and with stepwise increasing temperature. This methodical approach allows investigating more temperature steps. Furthermore, strong emphasis was placed on microstructure investigations of tested specimens in order to relate creep behaviour to possible changes in grain structure and phase stability. The compression creep experiments were also supported by high temperature C-ring creep tests, which allowed the microstructural characterization of typical creep damages after simultaneous tension and compression loading.

2. Experimental

The following sections summarize details on material, microstructural and creep characterization methods.

2.1. Material

The $Ba_{0.5}Sr_{0.5}Co_{0.8}Fe_{0.2}O_{3-\delta}$ (BSCF) material was provided by Fraunhofer-Institut für Keramische Technologien und Systeme (IKTS), Institutsteil Hermsdorf (formerly Hermsdorfer Institut für Technische Keramik e.V., HITK). The perovskite had been extruded into a tubular shape and sintered at 1130 °C for 2 h. The tubes of 15 mm outer diameter and 1 mm wall thickness were cut by IKTS into shorter sections of ~30 mm length. In order to investigate the grain size influence on creep behaviour, some specimens received an additional heat treatment at 1150 °C for 2 and 50 h. The chemical composition of the as-received BSCF was verified by SEM investigations, using energy dispersive X-ray spectroscopy (EDS) (Table 1).

2.2. Microstructural characterization

For microstructural investigations the samples were embedded in epoxy resin, ground on 800–4000 grit abrasive papers, and polished with diamond suspensions and pastes. The grain size determination was carried out with specimens first removed from the resin and then thermally etched for 30 min at 900 °C. Scanning electron microscope (SEM, LEO 440) and light microscope (Zeiss Axiomat) were used to document and analyze the microstructure.

Table 1
Chemical composition of as-received BSCF obtained by SEM-EDS (oxygen is excluded from quantification).

	Element				
	SrL	BaL	FeK	CoK	Total
wt%	29	38	6	27	100
at%	28	23	9	39	100

Porosity and grain morphology (grain size, aspect ratio) measurements were evaluated with the software AnalySIS©. The average porosity, measured from cross-sections of the tube walls, was $8 \pm 3\%$. Due to the extrusion process a thin layer with distinctly lower porosity ($4.7 \pm 0.5\%$) existed at the outer side of the tubes (Fig. 1). Although most pores had a size of up to 14 μm, some large pores with up to 250 μm in length could also be observed (Fig. 1). Additionally, in the as-received state a small amount of Cobalt oxide precipitations exists, resulting from the Co_3O_4 powder addition to the feedstock.[14] The grain size (defined by an equivalent circular diameter) in the as-received state was 29 ± 11 μm (Fig. 2). The additional heat treatment for either 2 or 50 h at 1150 °C resulted in an average grain size of 88 ± 33 and 140 ± 52 μm, respectively.

2.3. Creep tests

For compressive creep tests the upper and lower ends of the 30 ± 1 mm tubular specimens were ground and polished to obtain parallel surfaces. The creep tests were performed using Instron 1362 testing machines equipped with high temperature furnaces. One of the furnaces could be operated under vacuum conditions, which permitted creep testing under low

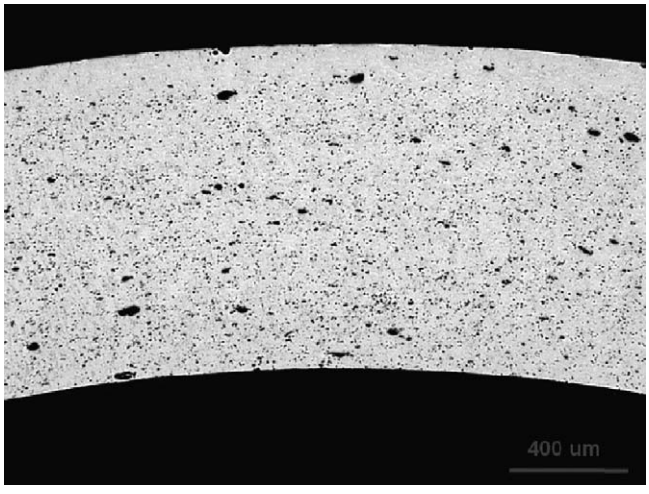

Fig. 1. Cross-section of a BSCF tube showing a thin layer of lower porosity near the outer surface and localized large pores.

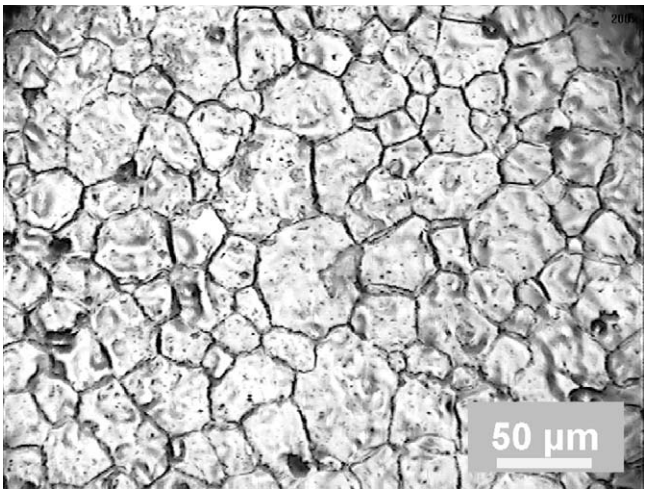

Fig. 2. Microstructure of the as-received BSCF material. Grain size 29 ± 11 µm.

oxygen partial pressure (4 and 2×10^{-6} mbar, corresponding to 2.13×10^{-2} to 1.05×10^{-9} MPa). For the creep tests in ambient air furnaces the oxygen partial pressure was assumed to be 1/5 of the measured absolute pressure.

The tubular specimens were mounted between a half-sphere (top) and plate (bottom), both machined from alumina. Alumina ceramics were also used for the upper pushing rod and the lower tubular support piston. The arrangement provided high temperature stability, stiffness and an uniaxial load train (Fig. 3). The displacement was measured inside the tubular specimen with a ceramic extension rod attached to a Linear Variable Differential Transformer (Sangamo, LVDT, range ± 1 mm, precision 1.25 µm). The load was determined with 1.5 and 10 kN load cells (Interface 1210 BLR and Interface 1210 ACK). The temperature was monitored during the test close to the outer specimen surface with a thermocouple.

The compressive creep experiments were performed with applied creep stresses of 20, 30 and 63 MPa. The tests were carried out at selected temperatures in the range 600–950 °C with

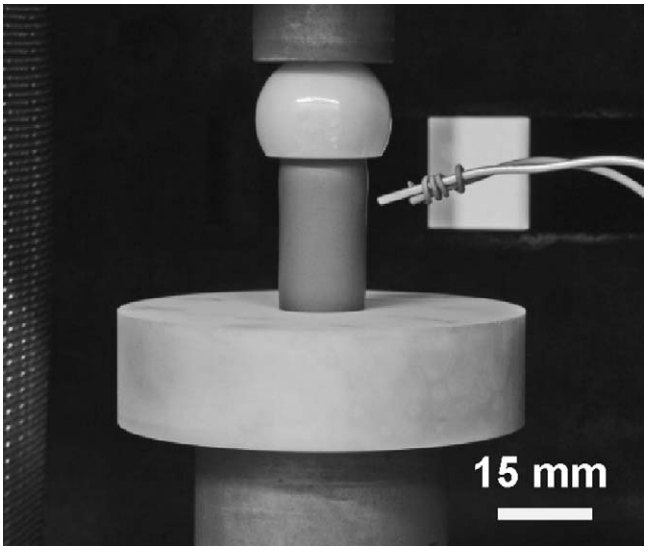

Fig. 3. Set-up of the compressive creep test.

increments between 25 and 100 °C. Before creep loading, the specimens were annealed at 850 °C for 24 h in the testing atmosphere to create an identical thermochemical starting situation for the tests. Note that this temperature is also in the same range proposed for the operation of the gas separation membranes.

After the 850 °C annealing, the samples were typically cooled down to 600 °C and kept at this temperature until steady state displacement was obtained. Thereafter the creep load was applied. The test at the given temperature was terminated either after 25 h or when displacement increase of 100 µm in creep was reached. Thereafter the load was removed, the sample was heated to the next testing temperature and after steady state displacement the creep load was applied again. This procedure was repeated in several steps until a temperature of 950 °C was reached.

Based on the experimentally measured displacement–time curves the compressive creep rates were derived for each temperature using a linear fitting routine. The resulting strain rates were mathematically described by a standard steady state creep equation[12]:

$$\dot{\varepsilon} = A\left(\frac{1}{d}\right)^{p} (pO_2)^m \sigma^n \exp\left(\frac{-E_a}{RT}\right) \quad (1)$$

where A is a constant, p the grain size exponent, m the oxygen partial pressure exponent, n the stress exponent, E_a the activation energy, R is the universal gas constant and d the grain size. The oxygen partial pressure pO_2, applied stress σ and temperature T are the input parameters from the experiments.

Based on Eq. (1), the data obtained during compressive creep tests permit a quantitative description of the creep behaviour and hence a more general prediction under various conditions. In the current analysis, a multi-parameter fitting routine was used with minimization obtained by a serial fitting routine, yielding an average value of activation energy and all the other relevant parameters in Eq. (1). To estimate the activation energy, a linear regression of $\ln \dot{\varepsilon} = f(1000/T)$ was used. The determination of the parameters n, m and p was based on linear regression of $\ln \dot{\varepsilon} = f(\ln \sigma)$, $\ln \dot{\varepsilon} = f(pO_2)$ and $\ln \dot{\varepsilon} = f(\ln 1/d)$, respectively. Note that since the procedure uses average values of the fitting parameters obtained by linear regression not all creep rate data are matching equally well.

However, information on deformation mechanisms and possible damage modes under tensile loading cannot be assessed from the axial compression tests with tubes. C-rings, which develop upon loading from outer to inner surface a transition from tensile to compressive stresses, can easily be machined from the tubular specimens. Hence, sections were cut from tubular specimens (width 10 mm, 5 mm gap) to obtain the final C-ring geometry (Fig. 4). Due to the low fracture load of BSCF in such specimen geometry (∼20 N) a dead-weight test with low load was performed. Again, alumina components were used for the loading jig (Fig. 5). Contrary to the fully instrumented creep tests under compression the C-ring experiment had the aim to reveal microstructural differences between tensile and compressive deformation. Note that the C-ring configuration results in a complex strain field with very high local strains.[15] Experimentally a dead load (6.7 N) was applied at room temperature and

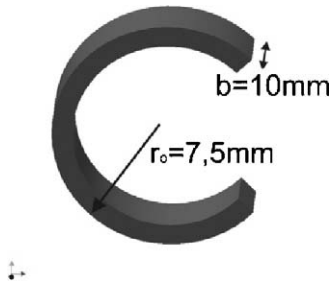

Fig. 4. Geometry of the C-ring test specimen.

then the specimen was heated up to 900 °C and kept with outages for a total time of 130 h. The C-ring tests were performed in laboratory air at ambient pressure.

3. Results and discussion

The basic experimental curves of creep displacement versus time verified in each case for the four tested parameter variations (temperature, oxygen partial pressure, mechanical stress and grain size) that stationary creep was reached. As an example experimental creep curves for as received BSCF (29 μm grain size) tested at 800 °C and 850 °C with 2×10^{-6} mbar oxygen partial pressure and 30 MPa compressive stress are shown in Fig. 6. It can clearly be seen that the data are well described by linear fits. As expected, the slope and hence the creep rate for 850 °C is larger than that for 800 °C. Summing up all displacements from each temperature an overall creep strain of ~8% has been reached during a typical test.

The individual creep test results can be conveniently grouped using graphical representations of individual parameters of Eq. (1). Fig. 7 displays the effect of oxygen partial pressure (a), grain size (b) and mechanical stress (c). Although the fitting procedure, which was carried out separately for each variable, introduces some uncertainty, equation (1) and the associated parameters in Table 2 permit a consistent description of the experimental data.

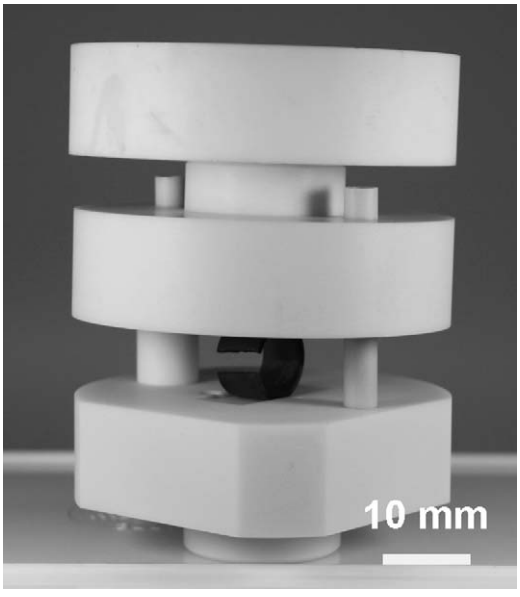

Fig. 5. Set-up of the C-ring creep test.

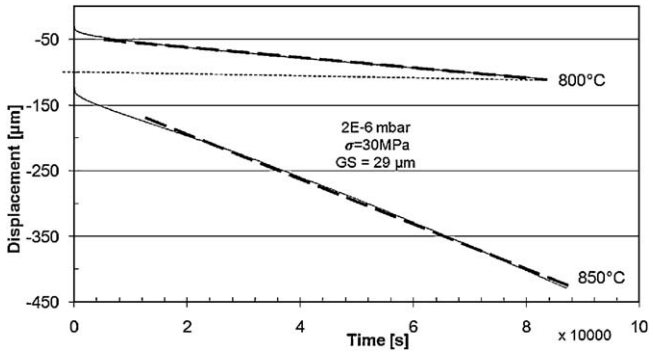

Fig. 6. Typical creep deformation plots.

Due to the complex behaviour of the experimental data in Fig. 7a the determination of one, averaging activation energy for the entire temperature range is not possible. In vacuum the activation energy determined for temperatures up to 800 °C from the Arrhenius plot is $E_a = 164 \pm 16$ kJ/mol. Note that fit parameters for creep tests in air below 800 °C have not been estimated since the creep rate appears to be rather constant in this range with a value of about 1.5×10^{-9} s^{-1}. However, in the high temperature range ($T > 800$ °C) the experimental data can be described for all oxygen partial pressures with one value of the activation energy: $E_a = 338 \pm 36$ kJ/mol. Note that the influence of the oxygen partial pressure at temperatures >800 °C is rather weak ($m = -0.14$). Displaced (shifted downwards) data point for 850 °C at air, well visible in Fig. 7a, will be considered in more detail in future works.

The influence of the applied compressive creep stress and the grain size dependence on creep rate for tests in air and temperatures above 800 °C are plotted in Fig. 7b and c, respectively. The data yield a stress exponent of $n = 1.7 \pm 0.5$ and a grain size exponent of $p = 1.7 \pm 0.2$.

Although different creep parameters have been reported for BSCF in Ref. 12 ($n = 0.76$, $m = -(0.57–0.67)$, $E_a = 228–320$ kJ/mol) the experimental data reported in that work can also be reasonably well described with the present creep parameters (Fig. 8). The particular data points are taken from Ref. 12 for comparison. This BSCF material might show variation due to production effects. Especially specimens geometry and grain size were different. Hence also other creep parameters (p, m, n and E_a) were also determined for this material in the respective literature work. However, the lines shown in the graph are results of own calculations using Eq. (1) with the parameters determined for the IKTS material investigated in house, but with correction for grain size of the material in the literature work (6.9 instead of 29 μm). This procedure was carried out to permit a better comparison and to see if the parameters are also valid for BSCF materials with other production parameters. In fact Fig. 8 shows that parameters determined on the basis of our experiments could quite well describe creep results for the material with similar chemical composition but different geometry, grain size and production parameters, for 5 MPa stress in the entire temperature range.

Table 2
Parameters of the creep equation determined using the experimental data.

T [°C]	pO_2	Average E_a [kJ/mol]	Average A [$m^{1.7}/(MPa^{1.56}$ s)]	n	m	p
$T>850$	All	338 ± 36	$(2.3 \pm 0.5) \times 10^{-3}$	1.7 ± 0.5	−0.14 ± 0.01	1.7 ± 0.2 (air)
$T<850$	20, 2×10^{-6} mbar	164 ± 16	$(8.7 \pm 2.6) \times 10^{-12}$			–
$T<850$	200 mbar (ambient pressure)	–	–	–	–	–

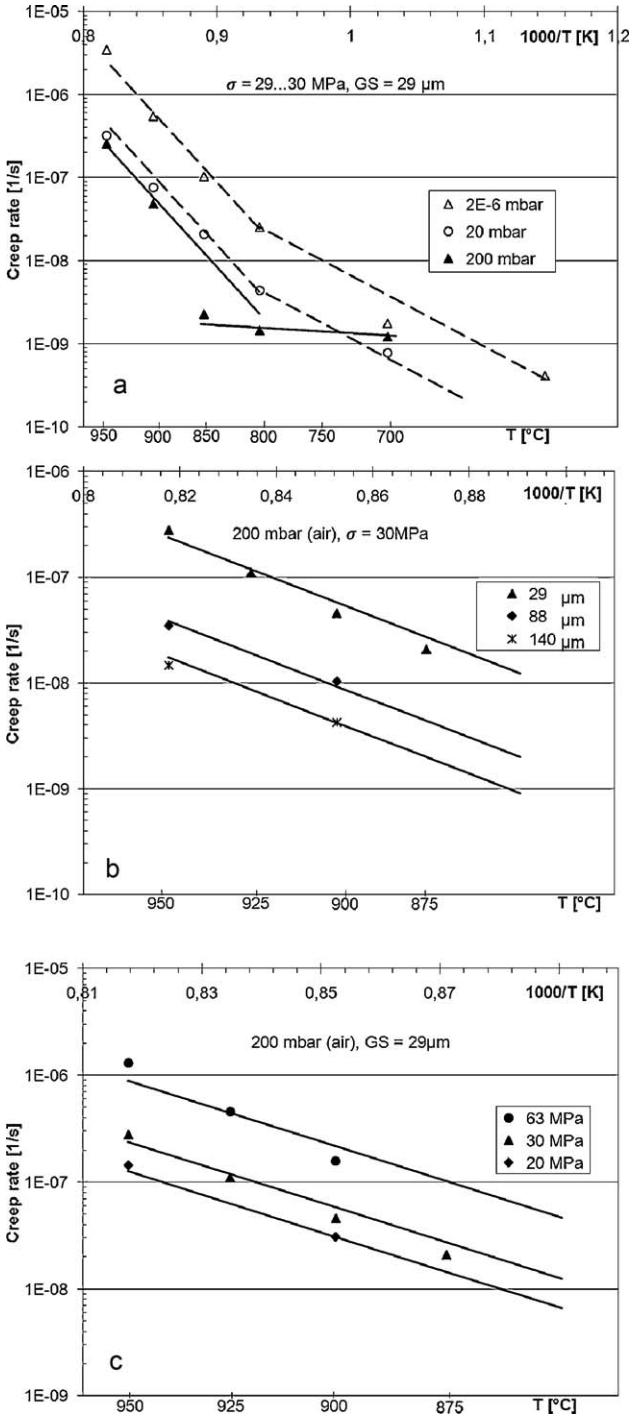

Fig. 7. Creep rates as a function of inverse temperature (a) partial pressure effect, (b) grain size, and (c) compressive stress effect (air).

Above 5 MPa reasonable agreement of the proposed creep law for temperatures >900 °C can be seen. Hence interpretation of the creep mechanisms from stress exponent and activation energy needs the microstructural aspects of creep to be taken into consideration.

Above ∼800–850 °C the creep rates in high vacuum (2×10^{-6} mbar) are about one order of magnitude higher than creep rates in air (Fig. 7a). Additionally, the results from the tests in air reveal a pronounced increase in slope at about 800 °C. This confirms qualitatively the findings of a previous investigation on BSCF,[12] where a change in slope of the temperature dependent strain rate data was recognized at ∼900 °C. A similar effect has been reported for $SrCo_{0.8}Fe_{0.2}O_{3-\delta}$ at 925 °C.[9] In Fig. 7a also a slight change in slope is visible for the data of the vacuum tests. The transition appears to happen at ∼800 °C. Although the transition temperatures are not fully consistent, the air result correlate with the observation that cubic BSCF becomes unstable in air at intermediate temperatures and gradually transforms to a hexagonal symmetry upon cooling.[16] Cubic and hexagonal BSCF polymorphs were observed to coexist below ∼850 °C, and the amount of the hexagonal polymorph was shown to increase at the expense of the cubic symmetry with decreasing temperature. It has also been suggested[17] that the phase transition temperature between the two perovskite polymorphs decreases with decreasing partial pressure of oxygen in agreement with the lower temperature for the change in creep rate slope under vacuum. Microstructural examinations suggest that the transition in the slope of the creep rate might be related with a transition from presence to absence of the hexagonal BSCF polymorph. The hexagonal phase was predominantly observed

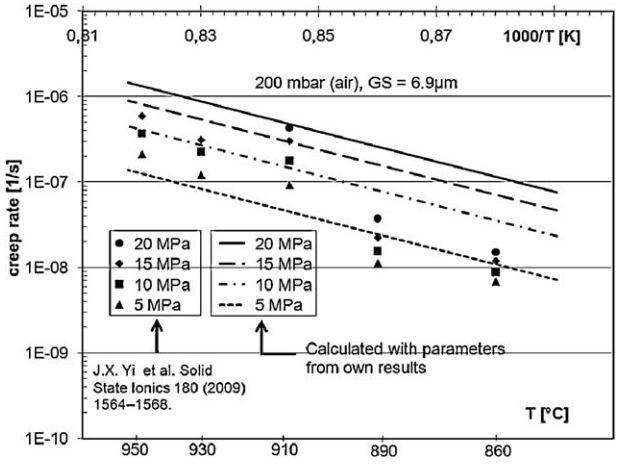

Fig. 8. Application of the creep equation parameters determined in the present work to the results reported in Ref. 12.

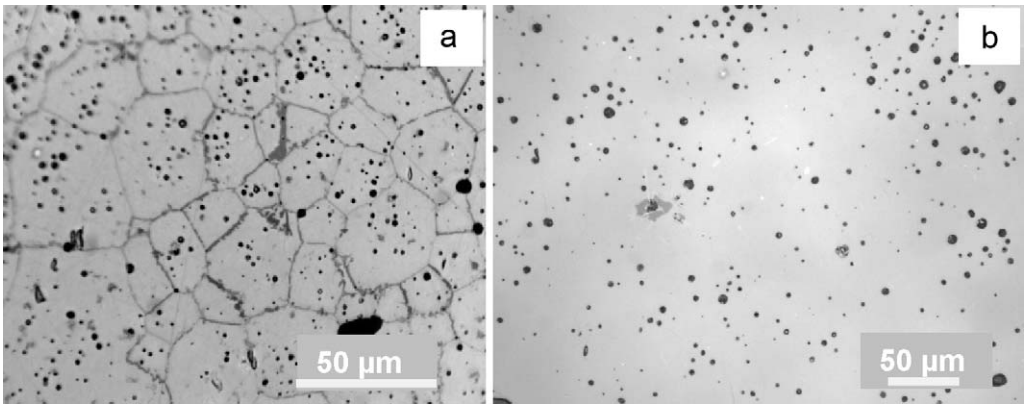

Fig. 9. LM micrographs of BSCF specimens (a) annealed 336 h at 800 °C and (b) followed by 24 h annealing at 950 °C.

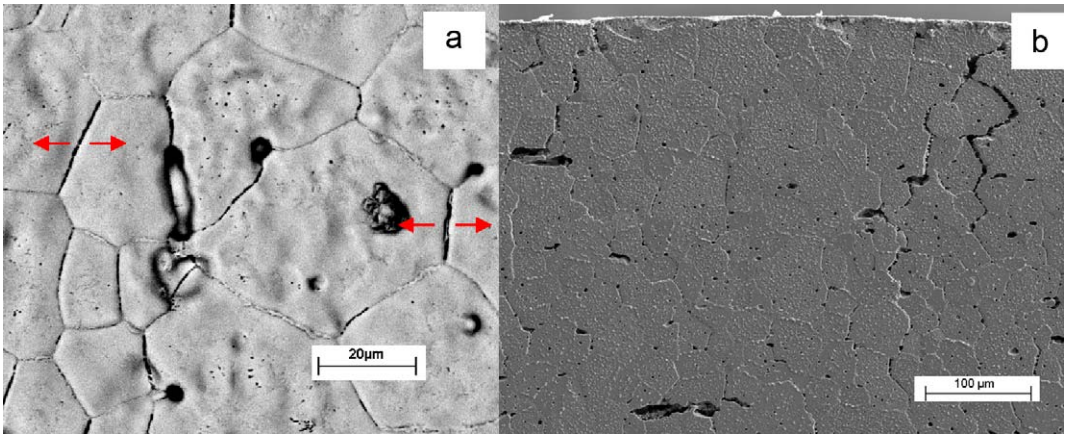

Fig. 10. SEM micrographs of specimens after creep testing (a) grain boundaries parallel to load direction are widened after a typical compressive creep test and (b) pores and microcracks after C-ring testing near the outer surface (tensile regime).

along the grain boundaries after annealing at 800 °C (Fig. 9a) but it disappeared above 850 °C. In fact, specimens annealed at 950 °C (Fig. 9b) did not show any grain boundary phase. In case of 2nd phase presence, SEM investigations (line-scan and EDS mapping) revealed iron depletion at the grain boundaries. More detailed, TEM investigations on grain boundary phase were performed in Ref. 16.

The microstructure of specimens after compressive creep testing showed several widened grain boundaries parallel to the loading direction (Fig. 10a, 900 °C, 2 h, 30 MPa). Note that size and aspect ratio of the grains remained unchanged.

The additionally carried out C-ring tests revealed severe creep damage in the tensile loaded outer specimen portion (Fig. 10b). The formation of pores and the opening of grain boundaries were visible in the tensile loaded areas. However, again size and aspect ratios of the grains agreed with the initial values. Similar to the tubular specimens loaded under pure compression the compressive loaded areas of the C-ring revealed slight opening of grain boundaries parallel to the applied stress direction (Fig. 10a).

Diffusion-controlled creep involving movement of vacancies via the lattice or along the grain boundaries is commonly referred to as Nabarro–Herring and Coble creep and characterized by a stress exponent of ~1. Also an inverse grain size exponent of two reflects Nabarro–Herring creep.[10] Here both stress and inverse grain size exponent had values of ~1.7 implying that the creep is governed by lattice diffusion. Combining the results of the fitted stress exponent of the creep equation with the microstructural observations supports the interpretation that diffusion initiated grain boundary separation is the dominating mechanism at high temperatures.

Extrapolation of the tensile creep rupture zone towards the load application line of the C-ring specimen can be used to derive a critical strain criterion. Within the damage zone identified by SEM investigations, the C-ring exhibits a remaining curvature change after the creep test, whereas outside of the damage zone no change in curvature could be measured. Analytical elastic calculations[15] of the strain field in a loaded C-ring revealed that damage by grain boundary separation occurs in regions where the elastic strains are higher than ~0.2%.

4. Conclusions

Between 600 °C and 850 °C the compressive creep rates of BSCF in air were almost constant but increased continuously up to 900 °C. Under reduced oxygen partial pressure (~2×10^{-6} mbar) the creep rates were about one order of magnitude higher than in air. An increase of grain size resulted in distinctly lower creep rates at temperatures above 850 °C in air, whereas at lower temperatures no significant effect on the creep rate could be observed.

The steady state compressive creep strain rates could be well described by a standard creep equation considering as exponential fitting parameters the influence of temperature, stress, oxygen partial pressure and grain size.

Microstructural investigations of the BSCF perovskite in the as-received state and after creep testing revealed independent of the testing condition no significant changes in grain morphology. However, in addition to the cubic perovskite symmetry the presence of a hexagonal phase was observed at the grain boundaries after annealing in air at 800 °C. The observed BSCF polymorph, which disappeared again at higher temperatures, appeared to be associated with the transition in creep behaviour.

Additionally carried out C-ring creep test revealed the formation of cavities along the grain boundaries normal to the tensile stresses that ultimately might lead to creep rupture. Note that, whereas under compressive loading creep strains of ∼1% per year might be sustained, a strain of ∼0.2% can already lead to damage under tensile loading.

Acknowledgements

This work was supported by the Initiative and Networking Fund of the Helmholtz Association, contract HA-104 ("MEM-BRAIN"). The authors would like to express their gratitude to T. Osipova, M. Braun and J. Mönch for the excellent experimental support of the creep tests. Special thanks go to Dr. R. Kriegel, IKTS-HITK, who provided the BSCF specimens for the present work and Dr. H.J.M. Bouwmeester for fruitful discussions on the creep behaviour of perovskite materials and the microstructural interpretation.

References

1. Czyperek M, Zapp P, Bouwmeester HJM, Modigell M, Peinemann K-V, Voigt I, et al. MEM-BRAIN gas separation membranes for zero-emission fossil power plants. *Energy Proc* 2009;**1**:303–10.
2. Shao ZP, Yang WS, Cong Y, Dong H, Tong JH, Xiong GX. Investigation of the permeation behavior and stability of a $Ba_{0.5}Sr_{0.5}Co_{0.8}Fe_{0.2}O_{3-delta}$ oxygen membrane. *J Membr Sci* 2000;**172**(1–2):177–88.
3. Sunarso J, Baumann S, Serra JM, Meulenberg WA, Liu S, Lin YS, et al. Mixed ionic-electronic conducting (MIEC) ceramic-based membranes for oxygen separation. *J Membr Sci* 2008;**320**(1–2):13–41.
4. Hendriksen PV, Larsen PH, Mogensen M, Poulsen FW, Wiik K. Prospects and problems of dense oxygen permeable membranes. *Catal Today* 2000;**56**:283–95.
5. Atkinson A, Ramos TMGM. Chemically-induced stresses in ceramic oxygen ion-conducting membranes. *Solid State Ionics* 2000;**129**:259–69.
6. Goretta KC, Park ET, Guan J, Balachandran U, Dorris SE, Routbort JL. Diffusional creep of $BaCe_{0.8}Y_{0.2}O_{3-alpha}$ mixed conductors. *Solid State Ionics* 1998;**111**(3–4):295–9.
7. Lein HL, Wiik K, Einarsrud MA, Grande T. High-temperature creep behavior of mixed conducting $La_{0.5}Sr_{0.5}Fe_{1-x}Co_xO_{3-delta}$ ($0.5 <= x <= 1$) materials. *J Am Ceram Soc* 2006;**89**(9):2895–8.
8. Majkic G, Wheeler LT, Salama K. Stress-induced diffusion and defect chemistry of $La_{0.2}Sr_{0.8}Fe_{0.8}Cr_{0.2}O_{3-delta}$ – Part 1 – creep in controlled-oxygen atmosphere. *Solid State Ionics* 2003;**164**(3–4):137–48.
9. Majkic G, Wheeler L, Salama K. Creep of polycrystalline $SrCo_{0.8}Fe_{0.2}O_{3-delta}$. *Acta Mater* 2000;**48**(8):1907–17.
10. Majkic G, Wheeler LT, Salama K. High-temperature deformation of $La_{0.2}Sr_{0.8}Fe_{0.8}Cr_{0.2}O_{3-delta}$ mixed ionic-electronic conductor. *Solid State Ionics* 2002;**146**(February (3–4)):393–404.
11. Thompson DR, Bool LE, Chen JC. *Oxygen enhanced combustion for NOx control. Final report*. Praxair, Inc.; 2004. Available online at http://www.osti.gov/bridge/.
12. Yi JX, Lein HL, Grande T, Yakovlev S, Bouwmeester HJM. High-temperature compressive creep behaviour of the perovskite-type oxide $Ba_{0.5}Sr_{0.5}Co_{0.8}Fe_{0.2}O_{3-\delta}$. *Solid State Ionics* 2009;**180**:1564–8.
13. Huang BX, Malzbender J, Steinbrech RW, Singheiser L. Discussion of the complex thermo-mechanical behavior of $Ba_{0.5}Sr_{0.5}Co_{0.8}Fe_{0.2}O_{3-\delta}$. *J Membr Sci* 2010;**359**(1-2):80–5.
14. Kriegel R, Kircheisen R, Töpfer J. Oxygen stoichiometry and expansion behavior of $Ba_{0.5}Sr_{0.5}Co_{0.8}Fe_{0.2}O_{3-\delta}$. *Solid State Ionics* 2010;**181**(1–2):64–70.
15. Bongartz K, Gyarmati E, Schuster H, Tauber K. The Brittle Ring Test: a method for measuring strength and young's modulus on coatings of HTR fuel particles. *J Nucl Mater* 1976;**62**(2–3):123–37.
16. Svarcova S, Wiik K, Tolchard J, Bouwmeester HJM, Grande T. Structural instability of cubic perovskite $Ba_xSr_xSr_{1-x}Co_{1-y}Fe_yO_{3-delta}$. *Solid State Ionics* 2008;**178**(35–36):1787–91.
17. Mueller DN, Souza RAD, Weirich TE, Roehrens D, Mayer J, Martin M. A kinetic study of the decomposition of the cubic perovskite-type oxide $Ba_xSr_{1-x}Co_{0.8}Fe_{0.2}O_{3-d}$ (BSCF) ($x = 0.1$ and 0.5). *Phys Chem Chem Phys* 2010;**12**:10320–8.